We are IntechOpen, the world's leading publisher of Open Access books
Built by scientists, for scientists

6,100
Open access books available

167,000
International authors and editors

185M
Downloads

Our authors are among the

154
Countries delivered to

TOP 1%
most cited scientists

12.2%
Contributors from top 500 universities

CLARIVATE ANALYTICS
BOOK CITATION INDEX
INDEXED

WEB OF SCIENCE™

Selection of our books indexed in the Book Citation Index in Web of Science™ Core Collection (BKCI)

Interested in publishing with us?
Contact book.department@intechopen.com

Numbers displayed above are based on latest data collected.
For more information visit www.intechopen.com

Chapter

Manipulating Light with Tunable Nanoantennas and Metasurfaces

Davide Rocco, Andrea Locatelli, Domenico De Ceglia, Andrea Tognazzi, Attilio Zilli, Michele Celebrano, Marco Finazzi, Antonio Ferraro, Roberto Caputo and Costantino De Angelis

Abstract

The extensive progress in nanofabrication techniques enabled innovative methods for molding light at the nanoscale. Subwavelength structured optical elements and, in general, metasurfaces and metamaterials achieved promising results in several research areas, such as holography, microscopy, sensing and nonlinear optics. Still, a demanding challenge is represented by the development of innovative devices with reconfigurable optical properties. Here, we review recent achievements in the field of tunable metasurface. After a brief general introduction about metasurfaces, we will discuss two different mechanisms to implement tunable properties of optical elements at the nanoscale. In particular, we will first focus on phase-transition materials, such as vanadium dioxide, to tune and control the resonances of dipole nanoantennas in the near-infrared region. Finally, we will present a platform based on an AlGaAs metasurface embedded in a liquid crystal matrix that allows the modulation of the generated second harmonic signal.

Keywords: tunability, metasurface, sensor, nonlinearity, dielectric

1. Introduction

Ultra-flat optical devices allow to manipulate and control propagating light by governing its phase, amplitude, and polarization states [1, 2]. Such properties, when optimized, can be employed to perform optical operations, such as beam steering and wavefront shaping.

This can find application in several fields such as microscopy, holography, imaging, communication, and sensing [3–6]. In traditional bulk optics, the signal modifications are obtained through refraction, reflection, absorption or diffraction of light [7–9]. The working principle is based on the wave propagation through various media with different refractive indices, which are optimized to obtain a well-defined optical path for specific operating wavelengths.

This mechanism was already known to ancient populations who used, for example, primitive lenses to focus the sunlight in tiny spots in order to ignite a fire. From then

on, several studies have led to an efficient optical control in several devices based on reflection and refraction, such as lenses, waveplates, and optical modulators [10–12]. Although a lot of them are still present in many commercial and technical products, their bulk nature is the main limiting factor for their integration and miniaturization in modern optical systems. In this context, a solution is offered by metasurfaces, which are artificial media composed by ensembles of subwavelength resonators (typically referred to as meta-atoms) that gained increasing attention in the last years [13–19]. Depending on the material composition, one can distinguish between metallic (or plasmonic) and dielectric metasurfaces. Both plasmonic and dielectric metasurfaces are based on the coupling between the meta-atoms to the incident electromagnetic wave. By properly designing the meta-atom shape, dimension and distribution, it is possible to implement functionalities that, in a much smaller volume, equal and even outmatch those offered by traditional bulky components, thus leading to a dramatic reduction of the footprint of the final photonic devices [20].

More specifically, devices such as metalenses, gradient phase shifters, vortex generation and hologram devices have been proposed and realized [21–26]. More recently, the focus shifted to the realization of dynamically reconfigurable metasurface [27, 28]. Differently from static metasurfaces, whose performances are defined and fixed by geometric constrains, in tunable metasurfaces the electromagnetic behavior can be modulated in response to an external stimulus, such as an electrical or optical signal. Several implementations have been proposed including ones exploiting thermal diffusion processes, optical tuning via nonlinear effects, and electron-induced phenomena [29–34]. A complete survey of these recent results is reported in [35].

Here, we review recent progresses for obtaining tunable functionalities in metasurfaces by concentrating on the material chosen as the constituent of the nanoresonators or surrounding them. The chapter is organized as follows: in Section 2 we introduce the concept of Phase-Change Materials (PCM). The PCM tuning mechanism relies on the modification of the refractive index across the phase transition. In particular, we will focus on vanadium dioxide, VO_2, and its transition from a dielectric to a metallic phase. We will demonstrate the tuning of the optical response of a plasmonic nano-resonator in the linear regime. Further, Section 3 is devoted to the reconfigurable mechanism in the nonlinear regime. More specifically, we report the tunable control of the Second Harmonic (SH) generated by an Aluminum Gallium Arsenide (AlGaAs) metasurface embedded in a liquid crystal matrix. Finally, in Section 4, we provide final remarks and an outlook on possible research directions.

2. Phase change material coupled with a plasmonic nanoantenna

In this section we report recent results concerning the use of the insulator-to-metal transition in a PCM to dynamically control the optical behavior of a nano-resonator [36, 37]. Let us underline that, in this paragraph, we will concentrate on a single nano-antennas. However, the reported results are fundamental for approaching the metasurface devices. In particular, we focus on VO_2 which is an extremely promising PCM for applications, since its insulator–metal phase transition occurs slightly above room temperature (at about 67°C) and can be induced thermally, electrically or optically [38, 39]. In [40] the authors perform electrical tuning of a plasmonic metasurface based on bow-tie antennas having the gap filled with VO_2 showing remarkable performances, however they do not provide general guidelines for the design of PCMs based resonators. To do so, in the following, we consider a plasmonic configuration: a

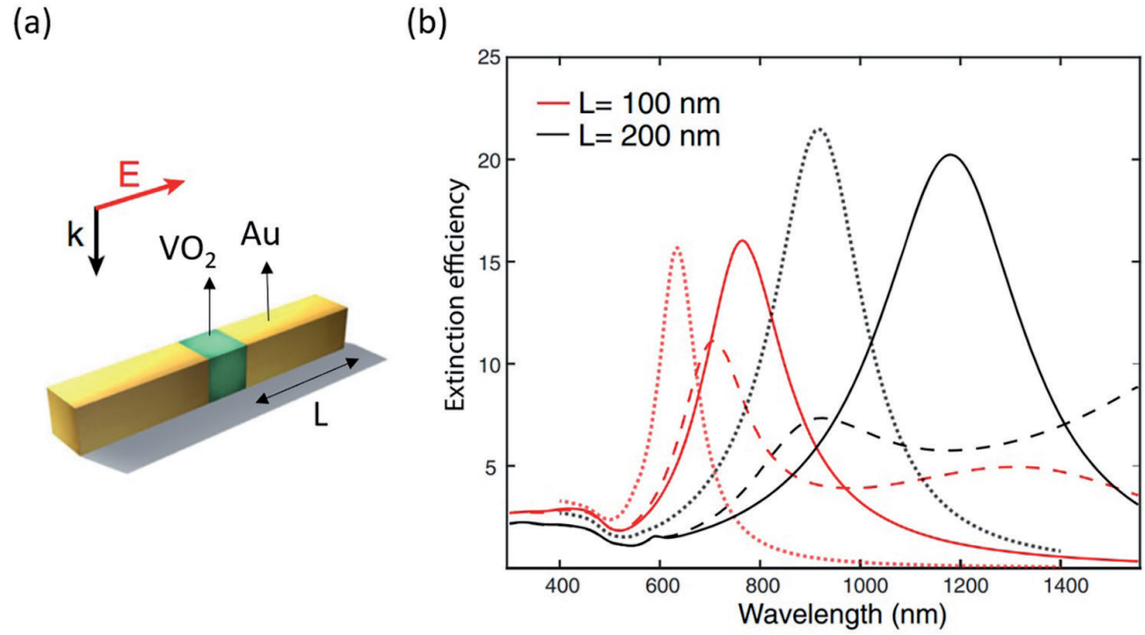

Figure 1.
(a) Sketch of the designed structure made by two gold arms with a gap filled with VO_2. (b) Extinction efficiency as a function of wavelength for different arm lengths. The continuous lines are associated with the PCM insulating phase; the dashed lines with the PCM metallic phase while the dotted lines correspond to the case where the gap is filled with air. The gap is fixed to 50 nm while the length L of the gold antenna is equal to 100 nm (red curves) and 200 nm (black curves), respectively.

single gold structure made of two arms with a square 50 × 50 nm^2 transverse section separated by a gap filled with VO_2, as shown in **Figure 1(a)** [41]. Let us highlight that the analysis with numerical simulations performed in Comsol Multiphysics v5.5—https://www.comsol.com— is useful to highlight some general considerations for the usage of PCMs in tunable optical systems which can be easily extended to other PCMs such as GeSbTe [42]. The proposed structure is placed in a homogenous surrounding material with refractive index equal to 1 (air). In the simulations, the gold nanoantenna is excited by a linearly polarized plane wave with electric field oriented along the long axis of the device, see **Figure 1**. We report – **Figure 1(b)** – the extinction efficiency for diverse arm length values above (dashed curves) and below (continuous curves) the critical transition temperature. For completeness, the case of air-filled gap is plotted in the figure with dotted curves. In the numerical investigation, we use the equilibrium optical constant at T = 30°C and T = 85°C for the insulating and metallic states, respectively. Few main aspects can be underlined by carefully observing the reported results.

Indeed, the optical properties are governed by the geometry of the structure. Firstly, when the arms lengths are increased, the resonances red-shift due to retardation effects, and broaden due to the increasing absorption of gold for wavelengths longer than 700 nm. Secondly, there is an evident arm length dependence of the shift between the resonances observed when the VO_2 inclusion is in either the metallic or the insulating phase. Therefore, the arm length represents a crucial parameter in these reconfigurable nanodevices. More specifically, the shift is smaller for shorter arm lengths. Moreover, the gap size can also affect the optical behavior. To investigate this dependence, in **Figure 2(a, b)** we report the extinction efficiency as a function of wavelength and gap size for the insulating and metallic phase, respectively. In these simulations the arms lengths are fixed to 200 nm. Regarding the insulating phase, we can notice a blue-shift of the resonant peak when the gap size is increased. This can be

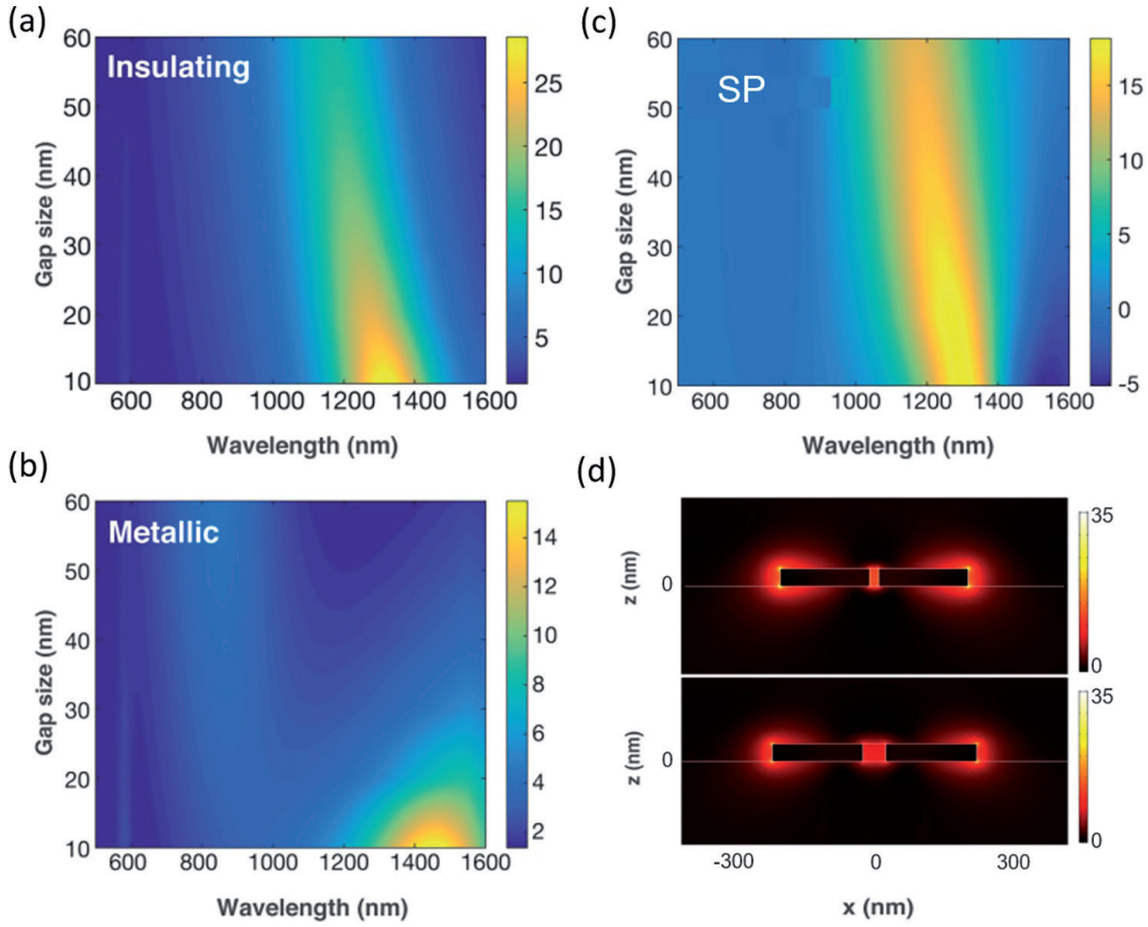

Figure 2.
Extinction efficiency σ_{ext} as a function of wavelength and gap size for the (a) insulating and (b) metallic phase of the VO_2 gap inclusion. The antenna arm length is 200 nm. (c) Switching parameter $\sigma_{ext}^{ins} - \sigma_{ext}^{met}$ as a function of wavelength and gap size. (d) Electric field enhancement ($|e|/E_0$) distribution at resonance for a structure with gap equal to 20 (top panel) and 50 nm (bottom panel).

understood by considering that, when the gap size is large enough, the two arms act as independent antennas. On the contrary, in the metallic state, a red shift of the less intense resonant peak as a function of the gap size can be seen. Intuitively, this can be explained by the fact that, when VO_2 is in the metallic phase, the entire device can be seen as a single antenna with increased length. To summarize all these results, we define the Switching Parameters, SP, as:

$$SP = \sigma_{ext}^{ins} - \sigma_{ext}^{met} \tag{1}$$

where σ_{ext}^{ins} and σ_{ext}^{met} represent the extinction efficiency for the VO_2 insulating or metallic phase, respectively. A plot of SP as a function of gap size and wavelength is reported in **Figure 2(c)**. The highest SP value is reached for small gaps, which better confine the electromagnetic field. **Figure 2(d)** elucidates the electric field distribution in the insulating phase for two different gap size values: 20 and 50 nm. One can clearly see that the electric field inside the gap is more uniform for the smaller value.

The SP can be evaluated also in the case of an asymmetric gap position. **Figure 3** shows the results obtained for this situation. The numerical predictions reveal that the maximum SP is achieved in the symmetric configuration, i.e., when the two arms are equal. Notably, the SP is not dramatically affected by small variations of

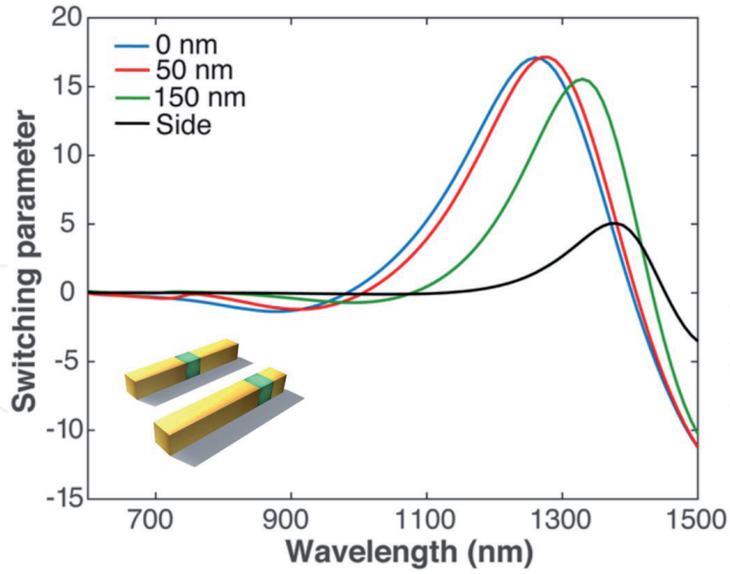

Figure 3.
Switching parameter as a function of the wavelength for different positions of the gap. The sketch represents the two conditions referred to in the legend as 0 nm (top) and 150 nm (bottom). In the legend, the number indicates the shift of the gap from the origin (center of the structure). The total length of the arms is 400 nm.

the gap position with respect to the perfectly symmetric condition. This means that the proposed device is robust with respect to fabrication defects that can alter the optimal geometrical design condition. Another important result is that the SP is not proportional to the volume of VO_2. This is of paramount importance since it allows to reduce the size of the device without reducing its functionality. Indeed, some recent works on PCM metasurfaces proved experimentally that a thin VO_2 film underneath dielectric resonators is sufficient to tune the behavior of a metasurface [43] and a metasurface of VO_2 nanocylinders can be employed to perform optical limiting [44].

To conclude, we have reported recent a recent example of a nanoresonator designed to maximize the metal–VO_2 near-field coupling to obtain tunable optical devices. The presented achievements may open new strategies for the implementation of optical structures whose behavior can be modulated by tuning external parameters, such as temperature, bias voltage and optical pump intensity [45, 46]. A metasurface composed by a repetition of the reported structure may benefit for even higher optical efficiency due to the resonance narrowing. Moreover, in the near future, this preliminary study related to the linear integration between nano-resonators and PCMs will also represent a guideline for nonlinear applications. For instance, in [47] the authors use the concept of PCM in the nonlinear regime and they numerically prove the tuning of second- harmonic generation (SHG) by gold metasurface made of split- ring resonators with a gap filled with GeSbTe alloy.

3. Liquid crystal-embedded nonlinear dielectric metasurface

In this section, we present recent results concerning the modulation of the nonlinear optical emission from dielectric metasurfaces excited in the infrared spectral region. As already mentioned before, despite the rapid advancements of nano-photonics and nanofabrication techniques, most of the up to now designed meta-structures exhibit a static behavior which is dictated by the fabrication process and cannot be changed [48–55]. However, the strong light–matter interaction in

dielectric materials can pave the way for a dynamic control of the optical response via the modification of their electromagnetic properties [56]. So far, different tuning mechanisms have been proposed, ranging from electrical to mechanical and thermal control [29, 32, 57] and as well PCM [58, 59]. In this context, the first demonstrations were carried out by considering the metasurface as a passive object where the output light wavelength is the same as the incoming one [60, 61]. However, dielectric materials such as GaAs and AlGaAs have also a strong nonlinear response of the second order with higher efficiency with respect to plasmonic nano-antenna [62]. In such high-refractive index materials it is thus possible to efficiently generate a signal at a different frequency (i.e. the double) than the input laser excitation [63, 64]. In this way, the metasurface acts already as an active device.

Recently, liquid crystals (LCs) emerged as excellent candidates for achieving dynamic light manipulation at the nanoscale mainly thanks to their high birefringence that can be governed by temperature or by an external electric field. Linear dielectric metasurfaces embedded in a LC matrix have been successfully implemented [65–67] where the molding of the light scattered from the structure depends on the orientation of the LC axis. However, the reconfigurable control of the nonlinear harmonic light emitted by metasurfaces embedded in LCs is still preliminary [68].

In the following, we review one possible implementation to obtain a SHG modulator by using a commercial LC as the immersion material of a metasurface made of AlGaAs nanodiscs placed over a low-refractive index substrate.

Let us consider the metasurface depicted in **Figure 4(a)** [69]. The structure is a periodic array of nanodiscs of height equal to 200 nm. The AlGaAs crystal axes are oriented as sketched in the inset of **Figure 4(b)**. The dielectric structure is covered by a LC whose director is kept in the plane of the metasurface. The employed LC is E7 which is quite popular in the display industry [70–72].

To demonstrate the modulation capability of the proposed device, nonlinear numerical simulations have been carried out. More specifically, the nonlinear SH signal coming from the metasurface has been calculated as a function of the lattice period p, the radius r of the nanocylinder and the polarization of the incident pump beam. The calculations have been performed using Comsol Multiphysics. The

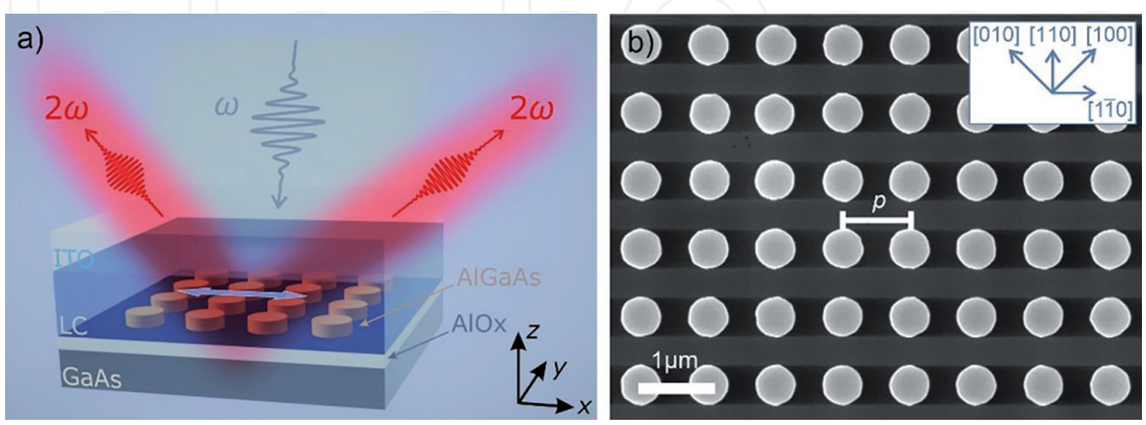

Figure 4.
(a) Sketch of the designed metasurface excited by the fundamental beam at ω. the unitary cell is constituted by a AlGaAs nanodisc that is placed on an Al_2O_3-GaAs substrate. An ITO superstrate is placed in view of future voltage-controlled implementations. The light blue arrow indicates the LC director parallel to the x axis. The harmonic generated at 2ω is measured as a function of the incident polarization. (b) Scanning electron microscopy image of the fabricated metasurface, with period p equal to 910 nm. Inset: The orientation of the AlGaAs crystalline axes.

AlGaAs nanodiscs are layered over an Al_2O_3 substrate. The refractive indices of the materials are the same as in Ref. [68]. For the modeling of the E7 LC we consider a homogeneous anisotropic dielectric material with ordinary (n_o) and extraordinary refractive index (n_e), respectively equal to 1.5 and 1.6 at the considered wavelength. Please note that this values slightly differ from the typically reported ones to account for imperfections in the device fabrication that lead to a lower anisotropy. In this way, the numerical results can mimic the realistic experimental conditions. The impinging beam is assumed to be a plane wave at normal incidence with a wavelength of 1551 nm. The SH emission is simulated in two steps. First, the field at the fundamental incident wavelength is evaluated. Then, the SH sources are computed in terms of current densities. More specifically, for the zincblende crystalline structure of AlGaAs the current density J_i can be computed as:

$$J_i(2\omega) = j\,\omega_{SH}\varepsilon_0\chi^{(2)}{}_{ijk}E_j(\omega)E_k(\omega) with i \neq j \neq k, \tag{2}$$

where i,j,k indicate the Cartesian axes, ε_0 the vacuum permittivity, $Ej(\omega)$ the jth component of the electric field at the fundamental frequency ω, $\chi^{(2)}{}_{ijk}$ the second-order susceptibility that we fix to 200 pm/V [64]. Please note that the nonlinear current densities are defined only in the dielectric medium because both the Al_2O_3 substrate and the LC have negligible $\chi^{(2)}$.

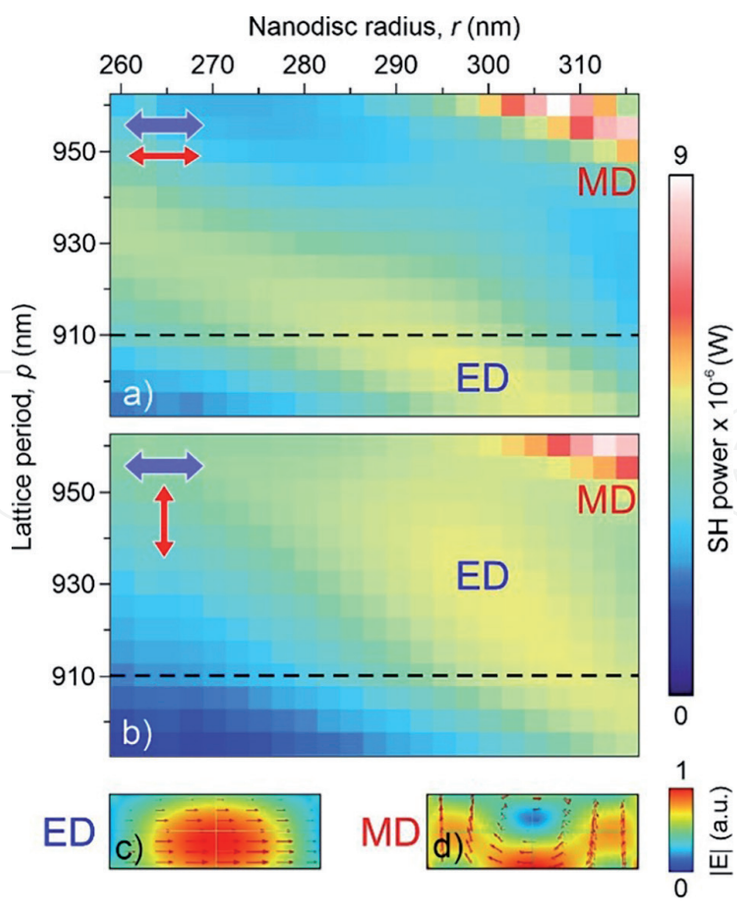

Figure 5.
Simulated SH emitted power as a function of metasurface period and nanodisc radius for linear pump polarization (red arrows) (a) parallel or (b) orthogonal to the LC director (blue arrows). Electric field distribution at (c) the electric (ED) and (d) magnetic dipolar (MD) resonance inside the nanodisc, x-z plane.

The obtained results are reported in **Figure 5**, where the predicted SH power maps computed in the backward direction are reported for the two considered incident beam polarizations, indicated as red arrows. In the simulations, the metasurface period p varies from 895 nm to 960 nm and the radius of the pillar r from 260 nm to 315 nm. **Figure 5(a)** and **(b)** highlight a strong dependence of the SH on the incident polarization. In particular, the numerical predictions reveal that the SH stem from an electric dipolar (ED) or magnetic dipolar resonance (MD) at the pump wavelength. The ED resonance is broader than the MD one, but it displays a more pronounced dependence on the relative orientation between the incident polarization and the LC director.

For instance, one can notice that, for p = 910 nm, (black dotted line in **Figure 5**), the ED resonances for the two incident light polarizations are observed at radii that differ by roughly 20 nm. Hence, the ED resonance is strongly modulated by the relative orientation between the incident light and the LC director. The latter is a crucial aspect for obtaining a metasurface that acts as a SH modulator. This promising consideration motivated the fabrication of such a device, as described in [69]. Briefly, the structure is fabricated by molecular-beam epitaxy on a non-intentionally doped GaAs wafer, with 200 nm layer of $Al_{0.18}Ga_{0.82}As$ on the top of an aluminum-rich substrate, which is later oxidized. Metasurfaces with varying cylinder radius in the range 260–315 nm and with period fixed at 910 nm have been obtained, as already reported in **Figure 4**. The metasurfaces are then embedded in a 12 μm-thick matrix of E7 LC following the procedure reported in [69].

The structures are then experimentally tested with the set-up already described in [64]. The source is an ultrafast laser with wavelength centered at 1551 nm which provides 160 fs pulses at 80 MHz repetition rate. The average excitation power is 10 mW that is associated with an average intensity on the sample of roughly 2 KW/cm^2 (peak intensity equal to 160 MW/cm^2) given a beam diameter of 25 μm. Please note that the metasurface acts as a diffraction grating for the SH signal. In particular, the first diffraction orders are supposed to be emitted with an angle of about 58° (accordingly to the Bragg's diffraction law).

The numerical aperture (NA) of the collection objective is equal to 0.85, hence only the first diffraction orders are detected by our set-up. The experimental Back-Focal Plane (BFP) images of the measured SH signal are reported in **Figure 6** as a

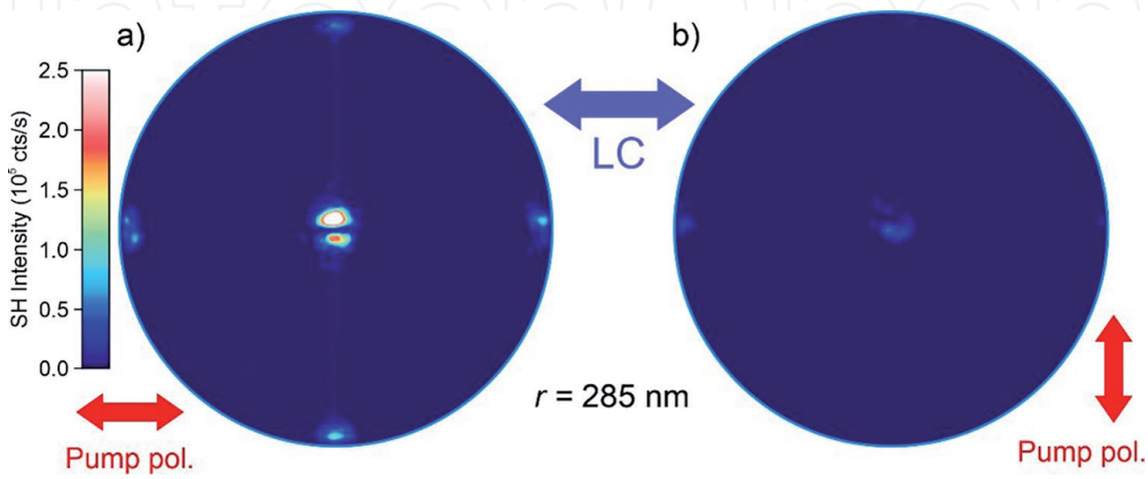

Figure 6.
Experimental BFP SHG maps of the proposed metasurfaces for the pump beam polarized (a) parallel or (b) orthogonal to the LC director. The red arrows represent the pump polarization while the blue arrow indicates the LC orientation.

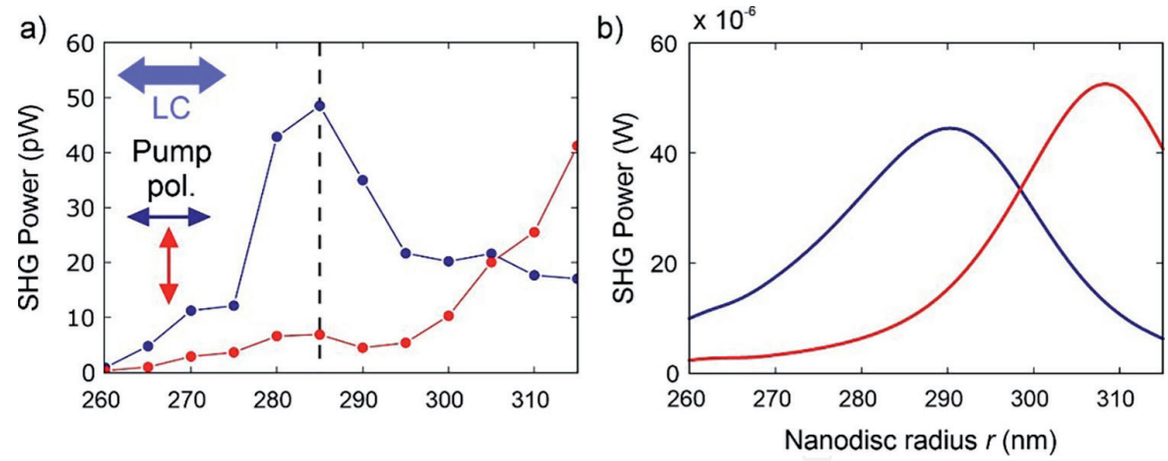

Figure 7.
Comparison between (a) experimental SH and (b) theoretical predictions as a function of the nanodisc radius for pump polarized parallel (blue line) or orthogonal (red line) to the LC director (light blue arrow). The vertical dashed black line marks the value of the nanodisc radius of the metasurface from which the BFP images reported in the previous figure were obtained.

function of the incident light polarization. Let us stress that the SH emission related to the first diffraction orders is at the edge of the NA and hence is partially cut off. However, it is clearly visible that the SH power is higher when the pump polarization is parallel to the LC director, see **Figure 6(a)**.

To validate and confirm this behavior, we acquired different BFP images by varying the nanodisc radius and the polarization of the incident light. **Figure 7** reports the obtained results compared to the numerical predictions. A shift in the SH peak is clearly visible when the incident polarization is switched from parallel (blue curve) to perpendicular (red curve) to the LC director. The experimental results and the theoretical predictions are in good agreement. We attributed the SH power trend to the shift of the ED resonance at the fundamental wavelength for the two considered excitations, see **Figure 5**. Importantly, for a metasurface with radius r = 285 nm the modulation of the SH power reaches the high value of about one order of magnitude, as highlighted by the dashed black line in **Figure 7**. In [69] the authors reported another structure where the LC director is always parallel to the (110) crystallographic axis. However, for the latter metasurface no significant SH modulation is expected and we will not further discuss this case here.

To summarize, for the first time to our knowledge, we have experimentally proven the modulation of the SH signal coming from an optimized dielectric metasurface covered by a liquid crystal matrix as a function of the incident pump beam polarization. Our experimental validation is achieved considering a fixed liquid crystal orientation (i.e. planar alignment). By switching the pump polarization, the refractive index felt by the meta-atoms as the upper medium modifies due to the anisotropic LC permittivity matrix. This variation shifts the wavelength position of the excited Mie resonances inside the dielectric and consequently the SH signal.

Importantly, for fixed incident wavelength and geometrical parameters of the metasurface, we obtain an order of magnitude enhancement in the emitted SH power when the incident pump polarization is switched from perpendicular to parallel to the LC director. Our experimental measurements, which are well reproduced by the numerical predictions, pave the way for the realization of nonlinear modulators in a scenario where the pump polarization is kept fixed and the liquid crystal anisotropy is controlled electrically or optically.

4. Conclusions

To conclude, in this chapter we have briefly discussed some of the recent progress in the field tunable nanophotonics. In particular, we focused on two recent approaches to attain efficient tuning of the meta-devices. We first discuss theoretical predictions about a specific phase-change material, VO_2, and how it can be used as a building block for reconfigurable meta-atoms. We have then reviewed the possibility of embedding dielectric metasurfaces in a liquid crystal matrix to achieve modulation of the nonlinear emitted light signal. These results clearly demonstrate how the control of the electromagnetic radiation can be achieved by well-optimized tunable metasurfaces. For practical applications, more efforts and solutions are needed for integrating reconfigurable metasurfaces within conventional electro-optical devices. The reduction of the fabrication costs is a key aspect to consider for a wide spreading of this technology. The versatility of nonlinear metasurfaces will certainly boost novel implementations in this research area.

Conflict of interest

The authors declare no conflict of interest.

Author details

Davide Rocco[1*], Andrea Locatelli[1], Domenico De Ceglia[1], Andrea Tognazzi[2], Attilio Zilli[3], Michele Celebrano[3], Marco Finazzi[3], Antonio Ferraro[4], Roberto Caputo[5] and Costantino De Angelis[1]

1 Department of Information Engineering, University of Brescia, Brescia, Italy

2 Department of Engineering, University of Palermo, Palermo, Italy

3 Department of Physics, Politecnico di Milano, Milano, Italy

4 Consiglio Nazionale delle Ricerche – Istituto di Nanotecnologia, Rende, Italy

5 Department of Physics, University of Calabria, Rende, Italy

*Address all correspondence to: davide.rocco@unibs.it

IntechOpen

© 2022 The Author(s). Licensee IntechOpen. This chapter is distributed under the terms of the Creative Commons Attribution License (http://creativecommons.org/licenses/by/3.0), which permits unrestricted use, distribution, and reproduction in any medium, provided the original work is properly cited. (cc) BY

References

[1] Kogelnik H. Imaging of optical modes-resonators with internal lenses. Bell System Technical Journal. 1965;**44**:455-494

[2] Luo X. Subwavelength artificial structures: Opening a new era for engineering optics. Advanced Materials. 2019;**31**:1804680

[3] Courjon D, Bainier C. Near field microscopy and near field optics. Reports on progress in Physics. 1994;**57**:989

[4] Eldada L. Optical communication components. Review of Scientific Instruments. 2004;**75**:575-593

[5] Frazão O, Santos JL, Araujo FM, Ferreira LA. Optical sensing with photonic crystal fibers. Laser & Photonics Reviews. 2008;**2**:449-459

[6] Deng Z-L, Li G. Metasurface optical holography. Materials today. Physics. 2017;**3**:16-32

[7] Golubenko G, Svakhin A, Sychugov V, Tishchenko A. Total reflection of light from a corrugated surface of a dielectric waveguide. Soviet Journal of Quantum Electronics. 1985;**7**:886

[8] Bolotovskiĭ B, Stolyarov S. Reflection of light from a moving mirror and related problems. Soviet Physics Uspekhi. 1989;**32**:813

[9] Blodgett KB. Use of interference to extinguish reflection of light from glass. Physical Review. 1939;**55**:391

[10] Reed G, Mashanovich G, Gardes F, Thomson D. Silicon optical modulators. Nature Photonic. 2010;**4**:518-526

[11] Drezet A, Cyriaque G, Ebbesen T. Miniature plasmonic wave plates. Physical Review Letters. 2008;**101**: 043902

[12] Hatakoshi GI, Tanaka SI. Grating lenses for integrated optics. Optics Letters. 1978;**2**:142-144

[13] Bukhari S, Vardaxoglou JY, Whittow W. A Metasurfaces review: Definitions and applications. Applied Sciences. 2019;**9**:2727

[14] Ding F, Pors A, Bozhevolnyi S. Gradient metasurfaces: A review of fundamentals and applications. Reports on Progress in Physics. 2017;**81**:026401

[15] Imani M, Gollub J, Yurduseven O, Diebold A, Boyarsky M, Fromenteze T, et al. Review of Metasurface antennas for computational microwave imaging. IEEE Transactions on Antennas and Propagation. 2020;**68**:1860-1875

[16] Hsiao H, Chu C, Tsai D. Fundamentals and applications of Metasurfaces. Small Methods. 2017;**1**:1600064

[17] Li A, Singh S, Sievenpiper D. Metasurfaces and their applications. Nanophotonics. 2018;**7**:989-1011

[18] Alaee R, Albooyeh M, Rockstuhl C. Theory of metasurface based perfect absorbers. Journal of Physics D: Applied Physics. 2017;**50**:503002

[19] Sung J, Lee G, Lee B. Progresses in the practical metasurface for holography and lens. Nano. 2018;**8**:1701-1718

[20] Qiu C, Zhang T, Hu G, Kivshar Y. Quo vadis, metasurfaces? Nano Letters. 2021;**21**:5461-5474

[21] Jiang Q, Jin G, Cao L. When metasurface meets hologram: Principle

and advances. Advances in Optics and Photonics. 2019;**11**:518-576

[22] Chen S, Liu W, Li Z, Cheng H, Tian J. Metasurface-empowered optical multiplexing and multifunction. Advanced Materials. 2020;**32**:1805912

[23] Luo X. Subwavelength optical engineering with metasurface waves. Advanced Optical Materials. 2018;**6**:1701201

[24] Yue F, Wen D, Xin J, Gerardot B, Li J, Chen X. Vector vortex beam generation with a single plasmonic metasurface. ACS Photonics. 2016;**3**:1558-1563

[25] Ma X, Pu M, Li X, Huang C, Wang Y, Pan W, et al. A planar chiral meta-surface for optical vortex generation and focusing. Scientific Reports. 2015;**5**:1-7

[26] Camacho-Morales R, Rocco D, Xu L, Gili V, Dimitrov N, Stoyanov L, et al. Infrared upconversion imaging in nonlinear metasurfaces. Advanced Photonics. 2021;**3**:036002

[27] Roy T, Zhang S, Jung I, Troccoli M, Capasso F, Lopez D. Dynamic metasurface lens based on MEMS technology. APL Photonics. 2018;**3**(021302):2018

[28] Shlezinger N, Alexandropoulos G, Imani M, Eldar Y, Smith D. Dynamic metasurface antennas for 6G extreme massive MIMO communications. IEEE Wireless Communications. 2021;**28**: 106-113

[29] Celebrano M, Rocco D, Gandolfi M, Zilli A, Rusconi F, Tognazzi A, et al. Optical tuning of dielectric nanoantennas for thermo-optically reconfigurable nonlinear metasurfaces. Optics Letters. 2021;**46**:2453-2456

[30] Rocco D, Gandolfi M, Tognazzi A, Pashina O, Zograf G, Frizyuk K, et al. Opto-thermally controlled beam steering in nonlinear all-dielectric metastructures. Optics Express. 2021;**29**:37128-37139

[31] Carletti L, de Ceglia D, Vincenti MA, De Angelis C. Self-tuning of second-harmonic generation in GaAs nanowires enabled by nonlinear absorption. Optics Express. 2019;**27**:32480

[32] Decker M, Kremers C, Minovich A, Staude I, Miroshnichenko A, Chigrin D, et al. Electro-optical switching by liquid-crystal controlled metasurfaces. Optics Express. 2013;**21**:8879-8885

[33] Schirato A, Mazzanti A, Zaccaria R, Nordlander P, Alabastri A, Della VG. All-optically reconfigurable plasmonic metagrating for ultrafast diffraction management. Nano Letters. 2021;**21**:1345-1351

[34] Pogna E, Celebrano M, Mazzanti A, Ghirardini L, Carletti L, Marino G, et al. Ultrafast, all optically reconfigurable, nonlinear nanoantenna. ACS Nano. 2021;**15**:11150-11157

[35] Yuan L, Fan S. Temporal modulation brings metamaterials into new era. Light: Science & Applications. 2022;**11**:1-2

[36] Appavoo K, Haglund RF. Polarization selective phase-change nanomodulator. Scientific Reports. 2014;**4**:1-6

[37] Wang H, Yang Y, H. and Wang L. Switchable wavelength-selective and diffuse metamaterial absorber/emitter with a phase transition spacer layer. Applied Physics Letters. 2014;**105**:071907

[38] Qazilbash Q, Brehm M, Chae BG, Ho PC, Andreev GO, Kim BJ, et al. Mott transition in VO2 revealed by infrared spectroscopy and nano-imaging. Science. 2007;**318**:1750-1753

[39] Kana JBK, Ndjaka JM, Vignaud G, Gibaud A, Maaza M. Thermally tunable optical constants of vanadium dioxide thin films measured by spectroscopic ellipsometry. Optics Communications. 2011;**284**:807-812

[40] Zhu Z, Evans P, Haglund R, Valentine J. Dynamically reconfigurable metadevice employing nanostructured phase-change materials. Nano Letters. 2017;**17**:4881-4885

[41] Tognazzi A, Locatelli A, Vincenti M, Giannetti C, De Angelis C. Tunable optical antennas using vanadium dioxide metal-insulator phase transitions. Plasmonics. 2019;**14**:1283-1288

[42] de Galarreta C, Sinev I, Alexeev A, Trofimov P, Ladutenko K, Carrillo SG, et al. Reconfigurable multilevel control of hybrid all-dielectric phase-change metasurfaces. Optica. 2020;**7**:476-484

[43] Tripathi A, John J, Kruk S, Zhang Z, Nguyen H, Berguiga L, et al. Tunable Mie-resonant dielectric Metasurfaces based on VO2 phase-transition materials. ACS Photonics. 2021;**8**:1206-1213

[44] Howes A, Zhu Z, Curie D, Avila J, Wheeler V, Haglund R, et al. Optical limiting based on Huygens' metasurfaces. Nano Letters. 2020;**20**:4638-4644

[45] Seo G, Kim B, Choi J, Lee Y, Kim H. Direct current voltage bias effect on laser-induced switching bistability in VO2-based device. Applied Physics Express. 2012;**5**:102201

[46] Tao Z, Zhou F, Han T, Torres D, Wang T, Sepulveda N, et al. The nature of photoinduced phase transition and metastable states in vanadium dioxide. Scientific Reports. 2016;**6**:1-10

[47] Guo K, Zhou K, Guo Z. Tunable second harmonic generation from bianisotropic plasmonic metamolecule via utilizing phase change materials. Journal of Applied Physics. 2020;**128**:133104

[48] Overvig AC, Shrestha S, Malek SC, Lu M, Stein A, Zheng C, et al. Dielectric metasurfaces for complete and independent control of the optical amplitude and phase. Light: Science and Applications. 2019;**8**:1-12

[49] Liu W, Li Z, Cheng H, Chen S. Dielectric resonance-based optical metasurfaces: From fundamentals to applications. Iscience. 2020;**23**:101868

[50] Genevet P, Capasso F, Aieta F, Khorasaninejad M, Devlin R. Recent advances in planar optics: From plasmonic to dielectric metasurfaces. Optica. 2017;**4**:139-152

[51] Albella P, Poyli M, Schmidt M, Maier S, Moreno F, Saenz J, et al. Low-loss electric and magnetic field-enhanced spectroscopy with subwavelength silicon dimers. Journal of Physical Chemistry C. 2013;**117**:13573-13584

[52] Shresta S, Overvig A, Lu M, Stein A, Yu N. Broadband achromatic dielectric metalenses. Light: Science Applications. 2018;**7**:1-11

[53] Zhao R, Xiao X, Geng G, Li X, Li J, Li X, et al. Polarization and holography recording in real- and k-space based on dielectric metasurface. Advanced Functional Materials. 2021;**31**:2100406

[54] Guo Z, Zhu L, Shen F, Zhou H, Gao R. Dielectric metasurface based high-efficiency polarization splitters. RSC Advances. 2017;**7**:9872-9879

[55] Zhang Q, Li M, Liao T, Cui X. Design of beam deflector, splitters, wave plates and metalens using photonic elements with dielectric metasurface. Optics Communication. 2018;**411**:93-100

[56] He Q, Sun S, Zhou L. Tunable/reconfigurable metasurfaces: Physics and applications. Research. 2019;**2019**:1-16

[57] Gutruf P, Zou C, Withayachumnankul W, Bhaskaran M, Sriram S, Fumeaux C. Mechanically tunable dielectric resonator metasurfaces at visible frequencies. ACS Nano. 2016;**10**:133-141

[58] Wang Y, Landreman P, Schoen D, Okabe K, Marshall A, Celano U, et al. Electrical tuning of phase-change antennas and metasurfaces. Nature Nanotechnology. 2021;**16**:667-672

[59] Zhang Y, Fowler C, Liang J, Azhar B, Shalaginov M, Deckoff-Jones S, et al. Electrically reconfigurable non-volatile metasurface using low-loss optical phase-change material. Nature Nanotechnology. 2021;**16**:661-666

[60] Komar A, Fang Z, Bohn J, Sautter J, Decker M, Miroshnichenko A, et al. Electrically tunable all-dielectric optical metasurfaces based on liquid crystals. Applied Physics Letters. 2017;**110**:071109

[61] Komar A, Paniagua-Domınguez R, Miroshnichenko A, Yu Y, Kivshar Y, Kuznetsov A, et al. Dynamic beam switching by liquid crystal tunable dielectric metasurfaces. ACS Photonics. 2018;**5**:1742-1748

[62] Gigli C, Leo G. All dielectric X(2) metasurfaces: Recent progress. Opto-Electronic. Advances. 2022;**210093**:1

[63] Marino G, Rocco D, Gigli C, Beaudoin G, Pantzas K, Suffit S, et al. Harmonic generation with multi-layer dielectric metasurfaces. Nano. 2021;**10**:1837-1843

[64] Gili V, Carletti L, Locatelli A, Rocco D, Finazzi M, Ghirardini L, et al. Monolithic AlGaAs second-harmonic nanoantennas. Optics Express. 2016;**24**:15965-15971

[65] Bohn J, Bucher T, Chong K, Komar A, Choi D-Y, Neshev D, et al. Active tuning of spontaneous emission by Mie-resonant dielectric metasurfaces. Nano Letters. 2018;**18**:3461-3465

[66] Zou C, Komar A, Fasold S, Bohn J, Muravsky A, Murauski A, et al. Electrically tunable transparent displays for visible light based on dielectric metasurfaces. ACS Photonics. 2019;**6**:1533-1540

[67] Hu Y, Ou X, Zeng T, Lai J, Zhang J, Li X, et al. Electrically tunable multifunctional polarization-dependent Metasurfaces integrated with liquid crystals in the visible region. Nano Letters. 2021;**21**:4554-456221

[68] Rocco D, Carletti L, Caputo R, Finazzi M, Celebrano M, De Angelis C. Switching the second harmonic generation by a dielectric metasurface via tunable liquid crystal. Optics Express. 2020;**28**:12037-12046

[69] Rocco D, Zilli A, Ferraro A, Borne A, Vinel V, Leo G, et al. Tunable second harmonic generation by an all-dielectric diffractive metasurface embedded in liquid crystals. New Journal of Physics. 2022;**24**:045002

[70] Schadt M. Liquid crystal materials and liquid crystal displays. Annual Review of Materials Science. 1997;**27**:305-379

[71] Bahadur B. Liquid crystal displays. Molecular crystals and liquid crystals. 1984;**109**:3-93

[72] Li J, Wen C, Gauza S, Lu R, Wu S. Refractive indices of liquid crystals for display applications. Journal of Display Technology. 2005;**1**:51